

On Real Fluid Flow Over Yawed Circular Cylinders¹

W. S. CHIU²

Research Assistant,
Department of Mechanical Engineering,
Massachusetts Institute of Technology,
Cambridge, Mass.

J. H. LIENHARD³

Professor of Mechanical Engineering,
University of Kentucky,
Lexington, Ky.

The equations for both the boundary layer and the outer potential flow over a yawed cylinder can be resolved into equations for the crosswise and spanwise velocity components. These components of the boundary layer are evaluated using Sears' method, and the separation point is found to be uninfluenced by the yaw angle. The potential-flow solutions for the spanwise and crosswise flows are added together to determine vortex patterns behind the cylinder. The approximate direct dependence of the Strouhal number upon the cosine of the yaw angle and/or the drag coefficient upon the square of the cosine, are verified. Experimental determinations of the Strouhal number and visualization of the flow pattern are consistent with the analysis.

Introduction

THIS study developed out of a research project aimed at understanding the wind excitation of power transmission lines. Our more restrictive purpose here will be that of describing the boundary layer, and (in relation with it) certain aspects of the vortex shedding from infinite, smooth, stationary, yawed, circular cylinders. Problems related to cylinder motion and the effects of outer strands of wound cables have also been studied but they will not be considered here.

¹ This work was supported jointly by the Bonneville Power Administration and the College of Engineering Research Division at Washington State University, Pullman, Wash.

² Formerly, Research Assistant, Mechanical Engineering Department, Washington State University.

³ Formerly, Associate Professor of Mechanical Engineering, Washington State University.

Contributed by the Fluids Engineering Division and presented at the Winter Annual Meeting, Pittsburgh, Pa., November 12-17, 1967, of THE AMERICAN SOCIETY OF MECHANICAL ENGINEERS. Manuscript received at ASME Headquarters, August 1, 1967. Paper No. 67-WA/FE-11.

The description of the inviscid flow in the cylinder wake is accomplished by adding a spanwise component of flow to the von Karman vortex street which appears as the crosswise component. To do this we must first learn whether or not the crosswise boundary-layer component is the same as in unyawed flow. This is particularly important with regard to separation since the vortex shedding frequency is related to the wake width and the base pressure, as Grove, et al. [1]⁴ and Roshko [2] have observed. A portion of this study is accordingly given to decomposing the boundary-layer equations into equations for the spanwise and crosswise flows and then solving these equations.

Two effects of the vortex shedding that have been proposed without proof in the past are: (a) That the vortex frequency decreases as the cosine of the yaw angle, β ; and (b) that the drag force decreases as $\cos^2 \beta$. Relf and Powell [3] obtained the latter result experimentally for the range $10^4 \leq Re_\infty \leq 10^6$, where⁵ $Re_\infty = 2U_\infty R/\nu$.

⁴ Numbers in brackets designate References at end of paper.

⁵ Symbols not explained in context are defined in the Nomenclature.

Nomenclature

a = spacing of vortices in upper or lower row, or an unspecified positive integer	Re_∞ = Reynolds number, $2U_\infty R/\nu$	z = coordinate normal to cylinder surface
b = spacing between upper and lower vortex rows	St = Strouhal number, $2f_v R/U_\infty$	α = angle between direction of flow and crosswise plane
C_D = drag coefficient, total drag force divided by $\rho U_\infty^2/2$	$U(x)$ = crosswise component of free-stream velocity at surface of cylinder	β = yaw angle, see Figs. 2 and 8
C_{Dp}, C_{Df} = pressure drag and friction drag coefficients based upon pressure drag and skin-friction forces	U_∞ = velocity of undisturbed flow	Γ = circulation of vortices in spanwise direction
$F = u/U_1$	U_1 = component of undisturbed flow in crosswise direction	Z = velocity component normal to $\xi - y$ plane
f_n = Blasius functions, defined by equation (8)	U' = velocity of vortex street with respect to undisturbed flow in crosswise direction	ζ = coordinate normal to $\xi - y$ plane
f_v = vortex shedding frequency	u = velocity component along cylinder surface in crosswise direction	$\eta = (\sqrt{Re_1}/R)z$
$G = v/V$	V = component of undisturbed flow in spanwise direction	$\theta = x/R$, see Fig. 2
g_n = functional coefficients for spanwise velocity, defined by equation (11)	v = velocity component in spanwise direction	μ = viscosity
$H = w\sqrt{Re_1}/U_1$	w = velocity component normal to cylinder surface	ν = kinematic viscosity, μ/ρ
n, m = summation indexes	x = coordinate along cylinder surface in crosswise direction	\bar{v} = velocity component in ξ -direction
p = pressure	y = coordinate parallel with cylinder surface	ξ = coordinate normal to cylinder, in plane of undisturbed flow
$p^+ = p/\rho U_1^2$		ρ = density of fluid
R = radius of cylinder		1 = general subscript indicating that U_∞ has been replaced with U_1 ; not applicable to g_n and f_n for $n = 1$

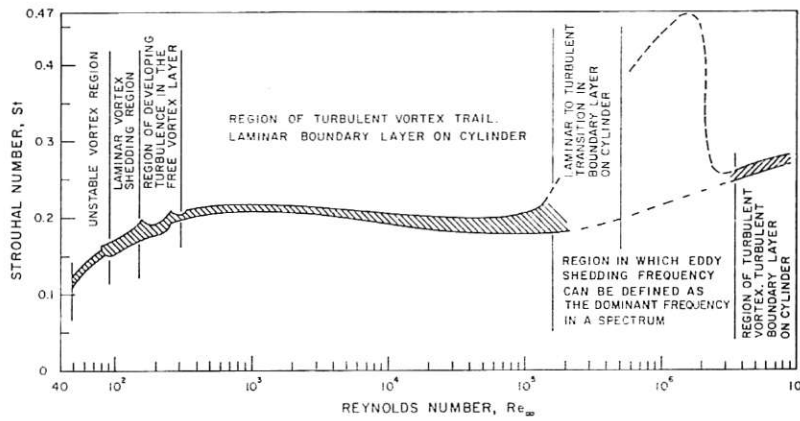


Fig. 1 Strouhal-Reynolds number relationship for unyawed circular cylinders as defined by existing data

Hanson [4] recently measured the effect of yaw angle upon the vortex frequency, f_v , behind a slender music wire in the range $40 \leq Re_\infty \leq 150$. He found that, for $\beta \leq 68$ deg, the relationship between the Strouhal and Reynolds numbers for unyawed cylinders (see Fig. 1)⁶ represented his data when the U_∞ in both St and Re_∞ was replaced with $U_\infty \cos \beta$. The representation was ragged at Re_∞ less than about 100 and good at the higher Re_∞ .⁷ Hanson also found that Re_∞ at the inception of unstable shedding did not increase quite as rapidly as $\cos^{-1} \beta$.

Prior investigations of the laminar boundary layer on yawed cylinders have been made by Wild [6] who used an integral method to solve the sweptback wing problem; by Cooke [7] who used an exact solution for the wedge flows; and by Sears [8] and Görtler [9]. Sears established, and Görtler extended, a general method for dealing with flows whose crosswise component of free-stream velocity is a polynomial in crosswise position. Schlichting [10] provides an excellent summary of these works.

These boundary-layer treatments predict that separation occurs at positions somewhat beyond where they are actually observed. This is because the descriptions become inaccurate in the neighborhood of the separation point. Nevertheless the qualitative behavior of such solutions is sound. Accordingly, we shall use Sears' method to determine how separation occurs on a yawed cylinder.

Calculation of the Boundary Layer

Fig. 2 shows the yawed, circular, cylinder configuration that we wish to describe. Under the following changes of variable:

$$\begin{aligned} u &= U_1 F(\theta, \eta) & \theta &= x/R \\ v &= V G(\theta, \eta) & \eta &= (\sqrt{Re_1}/R)z \\ w &= (U_1/\sqrt{Re_1})H(\theta, \eta) & p^+ &= p/\rho U_1^2 \end{aligned} \quad (1)$$

$$Re_1 = 2U_1 R/\nu$$

the crosswise and spanwise boundary-layer equations and the equation of continuity become

$$FF_\theta + HF_\eta = -p_\theta^+ + 2F_{\eta\eta} \quad (2)$$

$$FG_\theta + HG_\eta = 2G_{\eta\eta} \quad (3)$$

$$F_\theta + H_\eta = 0 \quad (4)$$

⁶ Fig. 1 is a "best estimate" which was made in reference [5] on the basis of the data of many previous investigators.

⁷ At 72 deg—the highest yaw angle—St was just twice what it should have been were it consistent with this representation. We wonder if this might not have been some effect related to vibration of the nonrigid wire.

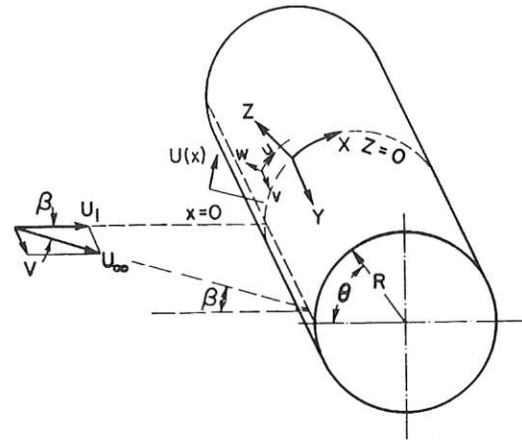


Fig. 2 Coordinate system

with boundary conditions

$$F = G = H = 0 \quad \text{at} \quad \eta = 0 \quad (5a)$$

$$F = G = 1 \quad \text{at} \quad \eta = \infty \quad (5b)$$

The crosswise component of the free-stream velocity is in this case

$$U(x) = 2U_1 \sin \theta = 2U_1 \sum_{n=1}^{\infty} \frac{\sin(n\pi/2)}{n!} \theta^n \quad (6)$$

so that $-p_\theta^+$, which can be written as RUU_z/U_1^2 , becomes

$$-p_\theta^+ = 4 \sum_{m,n=1}^{\infty} n \frac{\sin\left(\frac{n\pi}{2}\right)}{n!} \frac{\sin\left(\frac{m\pi}{2}\right)}{m!} \theta^{n+m-1} \quad (7)$$

Equations (2)–(5) with (7) comprise the system that we wish to solve for F , G , and H . In keeping with the method of Sears, we shall employ a stream function in the form of a Blasius' series

$$\psi = \frac{2RU_1}{\sqrt{Re_1}} \left\{ \sum_{n=1}^{\infty} \left[\frac{(n+1) \sin\left(\frac{n\pi}{2}\right)}{n!} \theta^n f_n(\eta) \right] - \theta f_i(\eta) \right\} \quad (8)$$

The crosswise and normal velocity components are then

$$F = \left[2 \sum_{n=1}^{\infty} \frac{(n+1) \sin\left(\frac{n\pi}{2}\right)}{n!} \theta^n f_n' \right] - 2\theta f_i' \quad (9)$$

and

$$H = - \left[2 \sum_{n=1}^{\infty} \frac{n(n+1) \sin\left(\frac{n\pi}{2}\right)}{n!} \theta^{n-1} f_n \right] + 2f_1 \quad (10)$$

while the spanwise velocity is expressed in terms of a different set of undetermined coefficients, as

$$G = \sum_{n=1}^{\infty} \theta^{n-1} g_{n-1}(\eta) \quad (11)$$

The substitution of equations (9) and (10) into equations (2) and (4) yields equations in the Blasius' functions, f_n . The evaluation of the f_n is well known and, in fact, has been done in a very general way by Tifford [11]. We have repeated this computation for f_1, f_2, \dots , and f_{11} and obtained values that differ slightly from Tifford's. Since the calculation of f_n is not difficult on a digital computer once $f_n''(0)$ is known, we shall only present a comparison of $f_n''(0)$ values with those computed from Tifford's functions, in Table 1. The resultant crosswise and normal velocity components are plotted in Figs. 3 and 4 for a somewhat larger range of variables than has been presented in the past.

It is of importance to note that the separation of the crosswise flow occurs when $\theta = 1.899$ rad or 108.8 deg regardless of the yaw angle. However, if the spanwise flow should separate before θ reaches this value, then we can no longer expect the inception of vortex shedding to be independent of yaw angle. Sears and Görtler present tables from which g_{n-1} can be obtained for $n = 1, 3, 5$, and 7 ; but this will give insufficient accuracy for large values of θ . Accordingly, we must extend this calculation before locating the separation point.

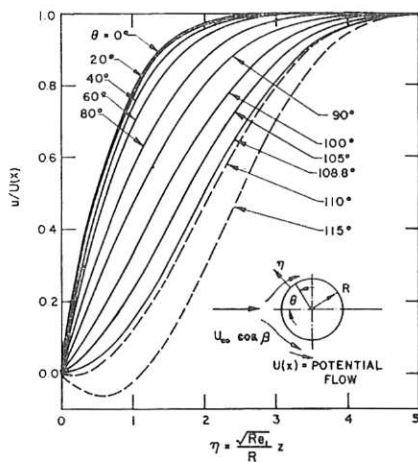


Fig. 3 Velocity profiles in crosswise direction

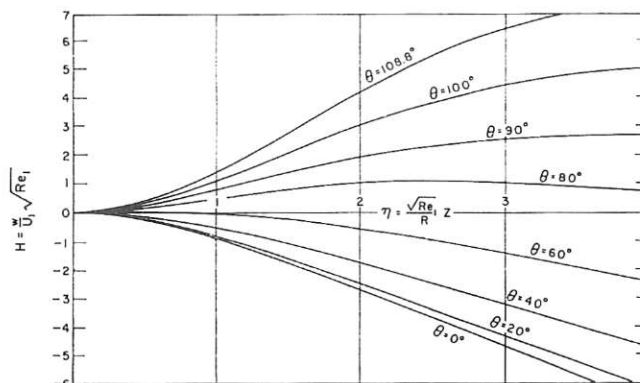


Fig. 4 Distribution of normal velocity component

Spanwise Velocity Distribution

The substitution of equations (9)–(11) into equation (3) gives

$$\sum_{n=1}^{\infty} \theta^{n-1} g_{n-1}'' = \sum_{n,m=1}^{\infty} \frac{(n-1)(m+1) \sin\left(\frac{m\pi}{2}\right)}{m!} \times$$

$$f_m' g_{n-1} \theta^{m+n-2} - f_1' \sum_{n=1}^{\infty} (n-1) \theta^{n-1} g_{n-1}$$

$$- \sum_{n,m=1}^{\infty} \frac{m(m+1) \sin\left(\frac{m\pi}{2}\right)}{m!} f_m g_{n-1}' \theta^{m+n-1}$$

$$+ f_1 \sum_{n=1}^{\infty} \theta^{n-1} g_{n-1}' \quad (12)$$

Equating the like coefficients of θ we get

$$g_{a-1}'' + f_1' g_{a-1} - f_1 g_{a-1}'$$

$$= \sum_{n,m=1}^{m+n=a+1} \frac{(m+1) \sin\left(\frac{m\pi}{2}\right)}{m!} [(n-1) f_m' g_{n-1} - m f_m g_{n-1}'] \quad (13)$$

where a is a positive integer. The boundary conditions on this family of second-order linear differential equations are:

$$g_n(0) = 0, \quad n = 1, 2, \dots; \quad g_0(\infty) = 1$$

$$g_n(\infty) = 0, \quad n \geq 1 \quad (5a)$$

Equation (13) becomes $g_0'' + f_1 g_0' = 0$ for $a = 1$. Its solution subject to the boundary conditions $g_0(0) = 0$ and $g_0(\infty) = 1$ is

Table 1 Comparison of initial values of $f_n''(0)$ computed by Tifford with those obtained in the present study

$f_n''(0)$	value of $f_n''(0)$ computed:	
	by Tifford	in present study
$f_1''(0)$	1.2326	1.2326407
$f_3''(0)$	0.7244	0.7245672
$f_5''(0)$	1.0320	1.0326583
$f_7''(0)$	2.0368	2.0422885
$f_9''(0)$	0.2801	0.3136514
$f_{11}''(0)$	67.6375	67.4999114

Table 2 Functional coefficients for spanwise velocity, g_n

η	ϵ_0	$-\epsilon_2 \times 10$	$-\epsilon_4 \times 10^2$	$-\epsilon_6 \times 10^3$	$-\epsilon_8 \times 10^4$	$-\epsilon_{10} \times 10^5$
0.	0.	0.	0.	0.	0.	0.
0.2	0.11495	0.17355	0.01188	0.08580	0.17810	0.51954
0.4	0.22792	0.34759	0.05225	0.16260	0.36034	1.03650
0.6	0.33849	0.51361	0.01797	0.21569	0.54932	1.54954
0.8	0.44616	0.67697	0.16675	0.23922	0.73379	2.06249
1.0	0.54692	0.72421	0.30766	0.24332	0.88445	2.57613
1.2	0.63833	0.77451	0.49470	0.26570	0.96797	3.06813
1.4	0.72001	0.77807	0.70591	0.34947	0.97402	3.47962
1.6	0.78325	0.73856	0.90850	0.52751	0.95667	3.73052
1.8	0.84620	0.66487	1.06807	0.80290	0.95178	3.76605
2.0	0.89131	0.56308	1.15830	1.14234	1.04668	3.60796
2.2	0.92569	0.46337	1.16743	1.48490	1.33699	3.37274
2.4	0.93939	0.36933	1.09984	1.76189	1.79393	3.23557
2.6	0.93865	0.26796	0.97290	1.91876	2.33970	3.25273
2.8	0.92868	0.19520	0.81095	1.93030	2.85326	3.78259
3.0	0.92852	0.12912	0.63875	1.80434	3.21344	4.44860
3.2	0.92542	0.08389	0.47651	1.57478	3.33923	5.16429
3.4	0.92536	0.05218	0.33730	1.28843	3.21138	5.70682
3.6	0.92406	0.03109	0.22689	0.99141	2.86974	5.90134
3.8	0.92301	0.01775	0.14522	0.71938	2.39213	5.67805
4.0	0.92291	0.00971	0.08853	0.49331	1.86647	5.08100
4.2	0.92277	0.00509	0.05145	0.32029	1.36722	4.23631
4.4	0.92259	0.00256	0.02852	0.19719	0.94263	3.29908
4.6	0.92236	0.00124	0.01510	0.11528	0.61303	2.40589
4.8	0.92222	0.00057	0.00763	0.06406	0.37669	1.64699
5.0	1.00000	0.00027	0.00368	0.03388	0.21907	1.00063

Table 3 Derivatives of functional coefficients for spanwise velocity, g_n'

η	ϵ_0'	$\epsilon_2' \times 10$	$\epsilon_4' \times 10^2$	$\epsilon_6' \times 10^3$	$\epsilon_8' \times 10^4$	$\epsilon_{10}' \times 10^5$
0.	0.57044	-0.86822	-0.05631	-0.43248	-0.88867	-2.59900
0.2	0.56957	-0.86216	-0.06913	-0.41816	-0.89606	-2.59465
0.4	0.56562	-0.82336	-0.14917	-0.33629	-0.92973	-2.57597
0.6	0.54862	-0.72774	-0.32373	-0.18783	-0.95118	-2.56056
0.8	0.52212	-0.57250	-0.57225	-0.04822	-0.86783	-2.57170
1.0	0.48349	-0.36683	-0.83191	-0.03280	-0.60846	-2.57446
1.2	0.43404	-0.13403	-1.01977	-0.22959	-0.21607	-2.38727
1.4	0.37649	0.09539	-1.06419	-0.63717	0.12701	-1.72170
1.6	0.31542	0.29214	-0.93216	-1.14639	0.18049	-0.72690
1.8	0.25846	0.43447	-0.64110	-1.57902	-0.20827	0.36557
2.0	0.19757	0.51259	-0.25128	-1.76285	-0.99000	1.11537
2.2	0.14755	0.52896	0.15609	-1.60356	-1.90622	1.08389
2.4	0.10594	0.49550	0.50483	-1.11953	-2.58602	0.15050
2.6	0.07311	0.42915	0.74369	-0.42791	-2.75692	-1.37534
2.8	0.04849	0.34727	0.85476	0.30552	-2.27418	-2.85854
3.0	0.03099	0.26430	0.85018	0.92487	-1.25875	-3.67955
3.2	0.01892	0.19203	0.76135	1.33057	0.01607	-3.32411
3.4	0.01113	0.12949	0.62609	1.49367	1.22722	-1.95036
3.6	0.00629	0.08382	0.47823	1.44647	2.12182	0.06385
3.8	0.00342	0.05163	0.34179	1.25649	2.57889	2.12584
4.0	0.00178	0.03030	0.22971	0.99861	2.61452	3.73044
4.2	0.00089	0.01697	0.14570	0.73460	2.33762	4.58308
4.4	0.00043	0.00907	0.08745	0.50397	1.89193	4.67335
4.6	0.00020	0.00463	0.04978	0.32413	1.40653	4.18290
4.8	0.00009	0.00226	0.02691	0.19618	0.96944	3.37514
5.0	0.00004	0.00105	0.01384	0.11206	0.62340	2.49145

$$g_0(\eta) = \frac{\int_0^\eta \exp \left[- \int_0^\eta f_1(\eta) d\eta \right] d\eta}{\int_0^\infty \exp \left[- \int_0^\eta f_1(\eta) d\eta \right] d\eta} \quad (14)$$

For $a = 2$, equation (13) becomes $g_1'' + f_1 g_1' - f_1' g_1 = 0$. This equation and the boundary conditions, $g_1(0) = g_1(\infty) = 0$, admits the trivial solution, $g_1(\eta) = 0$.

The $\sin(m\pi/2)$ elements in the right-hand side of equation (13) eliminate g_{n-1} from the equation for even or odd values of $(n - 1)$ when a is even or odd, respectively. Then, since $g_1 = 0$, equation (13) with $a = 4$ becomes an equation in g_3 only, whose solution is $g_3 = 0$. We can then see by induction that all other g with odd subscripts must also vanish.

The g with even subscripts have been obtained from successive numerical solutions of equation (13) for $a = 1, 3, \dots, 11$ beginning with the evaluation of g_0 using equation (14). Tables 2 and 3 present these values of g_n and g_n' . Fig. 5 displays the resulting spanwise velocity profiles computed with the aid of equation (11). These profiles show that the spanwise flow separates—that v_z vanishes on the wall—when θ exceeds 108.8 deg. The actual location of spanwise separation cannot be determined without computing a very large number of g_n . However, Fig. 6 illustrates that convergence is reasonably complete in terms up to g_{10} , as long as $\theta \leq 108.8$ deg.

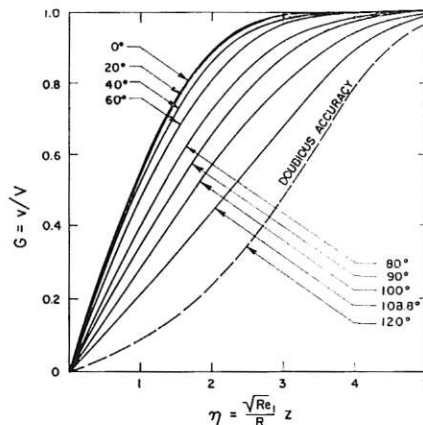


Fig. 5 Velocity profiles in spanwise direction

Spanwise separation is thus independent of β and would occur after the boundary has separated in the crosswise direction.

Effect of Yaw Angle Upon Vortex Frequency

Since the separation point has been proven independent of the yaw angle we can assume that the crosswise component of the vortex street is uninfluenced by spanwise flow. Neither the

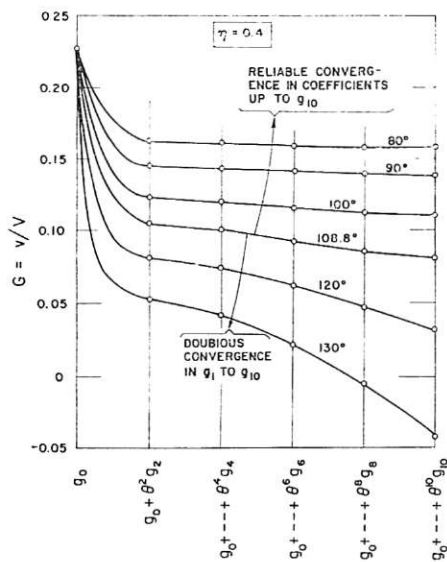


Fig. 6 Successive approximations to spanwise velocity distribution at various values of θ and at $\eta = 0.4$

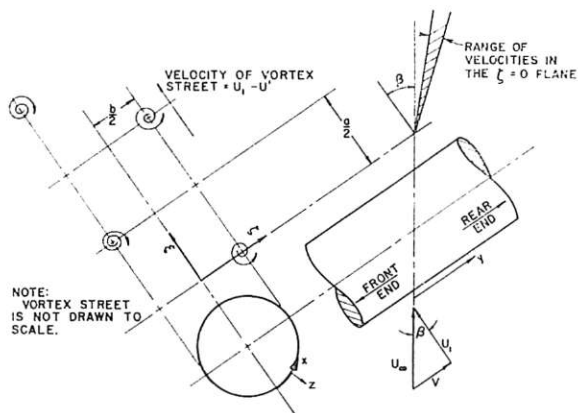


Fig. 7 Configuration of wake behind yawed cylinder

geometry of the street nor the circulation, Γ , of the vortices in the crosswise plane will change, Fig. 7. Vortices will thus be shed at a frequency corresponding with a velocity of $U_\infty \cos \beta$ over an unyawed cylinder. The correlation equation used by Hanson, namely,

$$\frac{2f_v R}{U_\infty \cos \beta} = St(2R(U_\infty \cos \beta)/\nu) = St(Re_1) \quad (15)$$

is thus vindicated. A Taylor series expansion of the right-hand side about Re_∞ gives

$$\frac{2f_v R}{U_\infty \cos \beta} \approx St(Re_\infty) - Re_\infty \left(\frac{dSt}{dRe} \right)_{Re_\infty} (1 - \cos \beta) \quad (16)$$

Inspection of Fig. 1 reveals that the second term on the right can be neglected above Hanson's range of interest and below the boundary-layer transition, especially when β is not very large. Thus, for a large range of practical interest,

$$f_v \approx (f_{v \text{ unyawed cylinder}}) \cos \beta \quad (17)$$

or

$$St \approx (St_{\text{unyawed cylinder}}) \cos \beta \quad (17a)$$

Grove, et al., have shown that below $Re_\infty \approx 300$ the thickness of the wake, which was constant at higher Re_∞ , is now a function of Re_∞ . This is the reason that Re_∞ begins to exert an influence on f_v as it decreases.

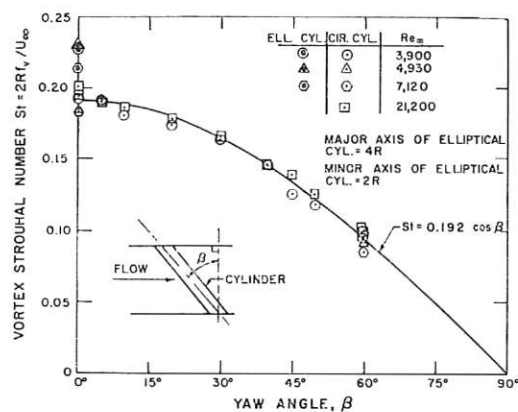


Fig. 8 Dependence of dimensionless vortex frequency upon yaw angle

It is not surprising that even equation (15) failed to correlate Hanson's results clearly at very low Re_1 since the regime of viscous flow ceases to take the form of a real boundary layer. The preceding proof of the independence of the separation point on yaw angle thus ceases to be meaningful.

A set of experiments by Chiu [12] in the range $3,900 \leq Re_\infty \leq 21,200$ verifies equation (17a) between $\beta = 0$ deg and 60 deg. These data, which were obtained with the help of a thermistor anemometer [12] in the wake of cylinders mounted in a water flume, are reproduced in Fig. 8. The reference value of St for the unyawed flow is only about 0.192. This is a little under the value of about 0.204 given by Fig. 1. The difference probably arises from minor sidewall effects in the flume [13].

Fig. 8 also displays data for an unyawed elliptical cylinder whose cross section corresponds with the flowwise cross section of a 60 deg circular cylinder. The Strouhal number based upon the minor diameter is a little above that for an unyawed circular cylinder, and much greater than $St \cos \beta$ for a cylinder of radius R yawed at 60 deg. This adds weight to our case by showing that flow over a yawed cylinder is not equivalent to flow over an unyawed cylinder that has the same elliptical cross section parallel to the flow.

Effect of Yaw Angle Upon Drag Coefficient

The drag coefficient, C_D , is the sum of a pressure drag component, C_{Dp} , and a frictional drag component, C_{Df} . For an unyawed cylinder, the pressure drag component constitutes more than half of the drag as long as vortices exist in the wake ($Re_\infty \lesssim 5$). As Re_∞ is increased from 300 to 10^4 , friction drag decreases from about one quarter to a negligible fraction of pressure drag (see, e.g., [5]).

The pressure drag coefficient computed by the classical von Karman theory [14] is

$$C_{Dp} = \frac{b}{2} \left[2.83 \left(\frac{U'}{U_\infty} \right) - 1.12 \left(\frac{U'}{U_\infty} \right)^2 \right] \quad (18)$$

for an unyawed cylinder in a flow for which $Re_\infty \geq 300$. The symbols b and U' designate the vertical spacing between vortex rows and the velocity of the vortex street with respect to the undisturbed fluid, respectively.

For a yawed cylinder, we wish to base the drag coefficient, $[C_{Dp}]_1$, upon the force in the crosswise direction and upon the flowwise velocity, U_∞ . Since both U' and U_∞ in equation (18) must be multiplied by $\cos \beta$ as the cylinder is yawed, there will be no net effect upon (U'/U_∞) . The only change will result from the U_∞^2 in the drag coefficient. Thus

$$[C_{Dp}]_1 = C_{Dp} \cos^2 \beta \quad (19)$$

The smaller friction drag component can be expressed as

$$C_{Df} = \left(\frac{1}{2} \rho U_\infty^2 \right)^{-1} \int_{x=0}^{\text{separation}} \mu (\partial u / \partial z)_{z=0} dx$$

or

$$C_{Df} = \text{Re}_\infty^{-1/2} [\text{function of } f_n''(0)] \quad (20)$$

for an unyawed cylinder. For a yawed cylinder, the U_∞ in C_{Df} and Re_∞ must be multiplied by $\cos \beta$. Thus

$$[C_{Df}]_1 = C_{Df} \cos \beta^{1/2} \quad (21)$$

which represents a slightly weaker influence of the yaw angle. We must thus write

$$[C_D]_1 \simeq C_D \cos^2 \beta; \quad \text{Re}_1 \geq 300 \quad (22)$$

as long as Re_1 and β do not simultaneously become very small and very large, respectively. When $\beta = 60$ deg and $\text{Re}_1 = 300$, for example, equation (22) will give a result that is about 21 percent high, but at $\beta = 60$ deg and $\text{Re}_1 = 1000$, the error is only about 5 percent.

Effect of Yaw Angle Upon Wake Behavior

The velocity components in a two-dimensional von Kármán vortex street are well known [14]. If we add the spanwise component to these components, we get a complete description of the potential flow in the wake

$$\Xi = U_1 + \frac{\pi\Gamma}{a} \left[\frac{\sinh \frac{\pi(2\zeta - b)}{a}}{\cosh \frac{\pi(2\zeta - b)}{a} - \cos \frac{2\pi\xi}{a}} - \frac{\sinh \frac{\pi(2\zeta + b)}{a}}{\cosh \frac{\pi(2\zeta + b)}{a} + \cos \frac{2\pi\xi}{a}} \right] \quad (23)$$

$$Z = -\frac{\pi\Gamma}{a} \left[\frac{\sin \frac{2\pi}{a} \left(\xi - \frac{a}{z} \right)}{\cosh \frac{\pi(2\zeta + b)}{a} + \cos \frac{2\pi\xi}{a}} + \frac{\sin \frac{2\pi\xi}{a}}{\cosh \frac{\pi(2\zeta - b)}{a} - \cos \frac{2\pi\xi}{a}} \right] \quad (24)$$

$$v = V = U_1 \tan \beta \quad (25)$$

where the velocity components, Ξ and Z , are in the ξ and ζ direction, respectively, Fig. 7. It is instructive to consider the angle, $\alpha = \tan^{-1}(V/\Xi)$, that the flow makes with the crosswise plane.

On the diametral plane in the flowwise direction (i.e., $\zeta = 0$)

$$\alpha = \tan^{-1} \left[\frac{U_1 \tan \beta}{U_1 - \frac{4.44\Gamma/a}{1 - (1/2) \cos^2(2\pi\xi/a)}} \right] \quad (26)$$

or if we note [14] that $2.22\Gamma/a = U'$:

$$\alpha = \tan^{-1} \left\{ \tan \beta \left/ \left[1 - \frac{2U'/U_1}{1 - (1/2) \cos^2(2\pi\xi/a)} \right] \right. \right\}$$

Thus, at points halfway between the upper and lower vortices, where $\xi = (2n + 1)a/4$, we obtain $\alpha = \tan^{-1}[\tan \beta / (1 - 2U'/U_1)]$. However, $f_v a/U_1 = 1 - U'/U_1$ and $a = b/0.281$. Accordingly, if we approximate³ $2R$ with b , then

³ Roshko [2] presents some data that indicate $1.10 < b/2R \leq 1.25$, depending upon Re_1 .

$$U'/U_1 \simeq 1 - 3.56 \text{St}(\cos \beta)^{-1}$$

and

$$\alpha \simeq \tan^{-1} [\sin \beta / (7.12 \text{St} - \cos \beta)], \quad \xi = \frac{(2n + 1)a}{4} \quad (26a)$$

Directly above and below the vortices, on the diametral plane, we likewise get

$$\alpha \simeq \tan^{-1} [\sin \beta / (14.24 \text{St} - 3 \cos \beta)], \quad \xi = na/2 \quad (26b)$$

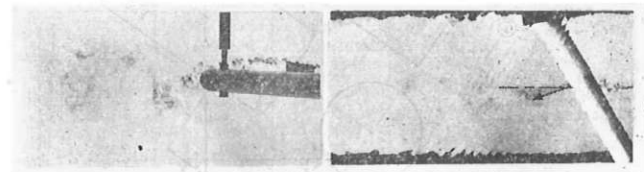
Equations (26a) and (26b) give for the $\beta = 35$ deg case shown in Fig. 7, $\alpha \simeq 44$ deg and 56 deg, respectively, when $\text{St} = 0.20$. The resulting range of velocities in the diametral plane is sketched in Fig. 7.

The motion of the vortex centers in the upper row can be obtained by setting $\xi = na$ and $\zeta = b/2$ [14]. Then the first term in equation (23) vanishes and

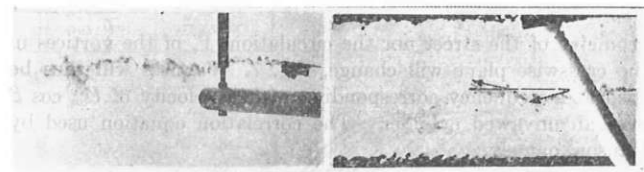
$$\alpha = \tan^{-1} \left[\frac{U_1 \tan \beta}{U_1 - \frac{\pi\Gamma}{a} \tanh \frac{\pi b}{a}} \right] = \tan^{-1} \left[\frac{\tan \beta}{1 - U'/U_1} \right] > \beta \quad (27)$$

Again, we can write $\alpha \simeq \tan^{-1} [\sin \beta / 3.56 \text{St}]$ so that for $\text{St} = 0.2$ and $\beta = 35$ deg, $\alpha \simeq 38.8$ deg. The vortex centers in the lower row will also have this same downstream direction, as a result of symmetry.

In the $\xi - y$ plane at $\zeta > b/2$ (a plane above the vortex centers), we must consider the bracketed term in equation (23). If



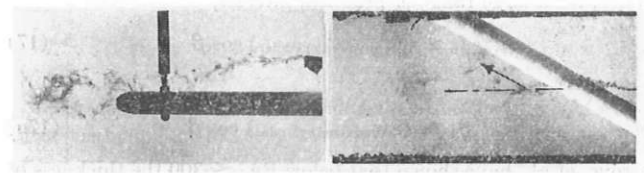
(a) $\beta = 20$ deg flow passing near cylinder surface



(b) $\beta = 20$ deg flow passing about 1 in. above cylinder



(c) $\beta = 60$ deg flow passing near cylinder surface



(d) $\beta = 60$ deg flow passing about 1 in. above cylinder

Fig. 9 Dye markings in wakes of a 1.5-in-dia yawed cylinder; $\text{Re}_\infty = 11,000$; flow from right to left; side view on left, top view on right

this term <0 then α will exceed β and the flow will deviate toward the rear or downstream end of the cylinder. After rearrangement this inequality becomes

$$\cos \frac{2\pi\xi}{a} < \left(\sinh \frac{\pi b}{a} \right) / \left(\sinh \frac{2\pi\zeta}{a} \right) \quad (28)$$

Condition (28) is satisfied for values of $\cos \frac{2\pi\xi}{a}$ that might be substantially <1 —that is, for fluid flowing through the region generally above the lower vortex tubes. Conversely, as the flow approaches the region directly above the upper vortex tubes, it will (at some point) have to deflect toward the front or upstream end of the cylinder.

Thus the vortex centers move in a straight line at an angle $(\alpha - \beta)$ with the free stream in the downstream, or rear, direction. When a fluid particle moves over the surface of the cylinder and separates, it first deviates to the front; then it deviates to the rear as the sheet upon which it rides rolls inside the vortex street. A particle thus moves in a corkscrew motion about the path of a vortex center. The fluid particles outside the vortex street meanwhile move in paths that oscillate in a nearly horizontal plane. Two sets of dye trails, for each of two yawed cylinders, illustrate this behavior in Fig. 9.

Conclusions

1 The spanwise separation point is independent of β , and it would occur beyond the crosswise separation point.

2 The Strouhal number and pressure drag coefficient can be evaluated for the crosswise component of flow, as though the spanwise flow did not exist. (The same would be true for the lift coefficient.)

3 Conclusions 1 and 2 become inaccurate near the low end of the vortex shedding regime ($Re_\infty < 100$) owing to the deterioration of the boundary layer at such low Re_∞ .

4 $[C_D]_1$ is somewhat greater than $C_D \cos^2 \beta$ as long as the skin friction is important since the influence of β upon C_{Df} is less than its influence upon C_{Dp} .

5 Particles in the cylinder wake describe counterrotating corkscrew paths within the upper and lower rows of the vortex street.

Acknowledgment

The authors are grateful to the R. L. Albrook Hydraulic Laboratory of the Washington State University College of Engineering Research Division for housing the experiments reported here and for maintaining the equipment. The WSU Computing Center and the M.I.T. Mechanical Engineering Department contributed the computer time used.

References

- 1 Grove, A. S., et al., "An Experimental Investigation of the Steady Separated Flow Past a Circular Cylinder," *Journal of Fluid Mechanics*, Vol. 19, Part 1, 1964, pp. 60-80.
- 2 Roshko, A., "On the Drag and Shedding Frequency of Two Dimensional Bluff Bodies," NACA TN 3169, 1954.
- 3 Relf, E. H., and Powell, C. H., "Tests on Smooth and Stranded Wires Inclined to the Wind Direction and a Comparison of the Results on Stranded Wires in Air and Water," British ARC, R and M 1917, Report #307.
- 4 Hanson, A. R., "Vortex Shedding From Yawed Cylinders," *American Institute of Aeronautics and Astronautics Journal*, Vol. 4, 1966, pp. 738-740.
- 5 Lienhard, J. H., "Synopsis of Lift, Drag, and Vortex Frequency Data for Rigid Circular Cylinders," College of Engineering Bulletin No. 300, Washington State University, Pullman, Wash., 1966.
- 6 Wild, J. M., "The Boundary Layer of Yawed Infinite Wings," *Journal of Aeronautical Science*, Vol. 16, 1949, p. 41.
- 7 Cooke, J. C., "The Boundary Layer of a Class of Infinite Yawed Cylinders," *Proceeding Cambridge Philosophical Society*, Vol. 46, 1950, p. 645.
- 8 Sears, W. R., "The Boundary Layer of Yawed Cylinders," *Journal of Aeronautical Science*, Vol. 15, 1948, pp. 49-52.
- 9 Görtler, H., "Die Laminare Grenzschicht am Schiebenden Zylinder," *Arch. Math.*, Vol. 3, Fasc. 3, 1952, pp. 216-231.
- 10 Schlichting, H., *Boundary-Layer Theory*, 4th ed., McGraw-Hill, New York, 1960.
- 11 Tifford, A. N., "Heat Transfer and Frictional Effects in Laminar Boundary Layers. Part 4: Universal Series Solutions," WADC Technical Report, 53-288, Part 4, Aug. 1954.
- 12 Chiu, W. S., "The Boundary-Layer Formation and Vortex Shedding on Yawed Cylinders," College of Engineering Bulletin No. 299, Washington State University, Pullman, Wash., 1966.
- 13 Lienhard, J. H., and Liu, L. W., "Locked-In Vortex Shedding Behind Oscillating Circular Cylinders, With Application to Transmission Lines," ASME Paper No. 67-FE-24.
- 14 Milne-Thompson, L. M., *Theoretical Hydrodynamics*, 4th ed., MacMillan, N. Y., 1960.